SLAC-PUB-13138

Technology of the LSST focal plane

P. O'Connor[a,*], J. Geary[b], K. Gilmore[c], J. Oliver[d], V. Radeka[a], P. Takacs[a]

[a]*Brookhaven National Laboratory, Upton, NY 11973, USA*
[b]*Harvard-Smithsonian Center for Astrophysics, Cambridge, MA 02138, USA*
[c]*Stanford Linear Accelerator Center, Menlo Park, CA 94025, USA*
[d]*Harvard University Laboratory for Particle Physics and Cosmology, Cambridge, MA 02138, USA*

Abstract

The Large Synoptic Survey Telescope, now in the research and development phase, will undertake a wide angle, deep survey of the entire southern sky starting in 2014. The survey database will support a wide variety of astrophysical investigations, with particular emphasis on elucidating the nature of dark energy. To achieve its science goals, LSST will incorporate a silicon-based focal plane with unprecedented size (3 Gpixel), speed (2 s readout), and sensitivity (high QE over 350–1000 nm wavelength). The technologies to be used in the LSST camera are described, with an emphasis on the silicon sensors and readout electronics.

1. Introduction

Recent studies in observational cosmology have produced strong evidence for a coherent model that describes the composition and evolution of the universe at the largest scales. Building on the key results of the Big Bang theory, researchers have made increasingly precise measurements of its main parameters using ground- and space-based telescopes with advanced detectors. Observations of the cosmic microwave background (CMB), the distribution of matter at large (10^8 light-year) scales, the kinetics of gravitationally bound systems, and the redshift–luminosity relationship of supernova "standard candles" are well fit by a concordance model known as "cold dark matter with cosmological constant" (ΛCDM). The parameters of this model that are now known to better than 10% include the present value of the Hubble constant, the temperature of the CMB blackbody radiation, the spatial flatness and total mass-energy density of the universe Ω_{tot}, and the baryonic matter fraction Ω_{B} [1]. Further analysis leads to the surprising conclusion that the dominant constituents of the universe are dark matter (DM; 23%) and dark energy (DE; 73%). The former is a type of clustered, non-baryonic matter that interacts purely gravitationally and has never been detected in any earthbound laboratory. Dark energy is a yet more enigmatic substance that exerts negative pressure, which has caused the universe's expansion rate to accelerate in the most recent epoch.

Although ΛCDM provides a self-consistent cosmological model with good fit to observations, its most prominent constituents do not fit into the rest of physics. Therefore, many new experimental studies have been proposed to investigate the physical nature of dark matter, determine how it is distributed in space now and in the past, and to elucidate the nature of dark energy and its variation with cosmic time.

2. Observational probes of dark energy

Dark energy leaves its imprint on the universe by affecting the expansion history and the rate of formation of large-scale structure. Optical surveys can detect several signatures of dark energy, which together can constrain its fundamental physical parameters.

2.1. Supernovae

Convincing evidence for dark energy initially came from a study of the distance–luminosity relationship of Type Ia supernovae, from which it was discovered that the expansion rate of the universe is accelerating [2]. The

*Corresponding author.
E-mail address: poc@bnl.gov (P. O'Connor).

Submitted to Nuclear Instrumentation and Methods (NIM) A

Work supported in part by US Department of Energy contract DE-AC02-76SF00515

absolute peak brightness of such supernova is known with high accuracy, and a measurement of the luminosity distance of many supernovae across a wide range of redshift gives a direct measure of the change in the Hubble parameter over time.

2.2. Weak gravitational lensing (WL)

One novel technique that can be used to measure the distribution of mass in the universe is WL [3]. Unlike strong lensing, where deflection of light by the gravitational field of a massive body can lead to multiple images or luminous arcs, weak lensing measures the differential deflection of light bundles by inhomogeneous gravitational fields. These tidal gravitational fields distort the shapes of distant sources, from which the intervening mass distribution can be determined. Fig. 1 depicts the characteristic tangentially oriented induced ellipticity of shapes by a point-like gravitational lens. Since the distant galaxies used as sources have intrinsic ellipticities, the technique is most effective when the shapes of large numbers of sources can be analyzed. One assumes that the intrinsic alignments are random, and that correlations in the observed shapes are due to WL. Clearly, the quality of the WL analysis is dependent on the size of the statistical sample and on control of systematic errors caused by distortions in the optical system.

When combined with redshift measurements of the background sources, weak lensing can give a tomographic reconstruction of mass vs. cosmic time. Since it is sensitive to the gravitational fields of both normal and dark matter, it provides a powerful probe of structures in the universe and the influence of dark energy on the growth of structure.

2.3. Galaxy and galaxy cluster statistics

Luminous galaxies and galaxy clusters can be considered to trace the distribution of dark matter, the large-scale statistical features of which are robustly predicted within any cosmological model. The spatial density and distribution of mass-selected galaxy clusters is sensitive to dark energy through its effect on the time evolution of the expansion rate and growth of structure through gravitational amplification of primordial density fluctuations.

Features in the matter power spectrum, such as baryon acoustic oscillations arising from pressure waves in the coupled baryon–photon plasma in the early universe [4], can be used as CMB-calibrated "standard rulers" which provide a geometric complement to the luminosity–distance methods for determining the time evolution of the expansion rate.

3. The Large Synoptic Survey Telescope (LSST) Project

LSST [5] will be a large, wide-field ground-based telescope designed to obtain sequential images of the entire visible sky every few nights from an observing site in northern Chile. The optical design (Fig. 2) involves a three-mirror system with an 8.4 m primary, which feeds three refractive correcting elements inside a camera, providing a 10 $\deg^2$ field of view sampled by a 3.2 Gpixel focal plane array. The total effective system throughput defined as the product of aperture and field of view, $A\Omega = 318\,\mathrm{m}^2\,\deg^2$, is nearly 2 orders of magnitude larger than that of any existing facility. The survey will yield contiguous overlapping imaging of 20,000–23,000 $\deg^2$ of sky in six optical bands. Wavefront sensors (see Table 1) in the focal plane provide feedback to an active alignment system, which controls the position and surface figure of the major elements of the optical system.

The LSST's 10-year survey mission will be carried out using a sophisticated scheduling algorithm that establishes a set of target fields each night based on atmospheric conditions, lunar phase, moving and transient object tracking, and a ranked set of science objectives. A detailed,

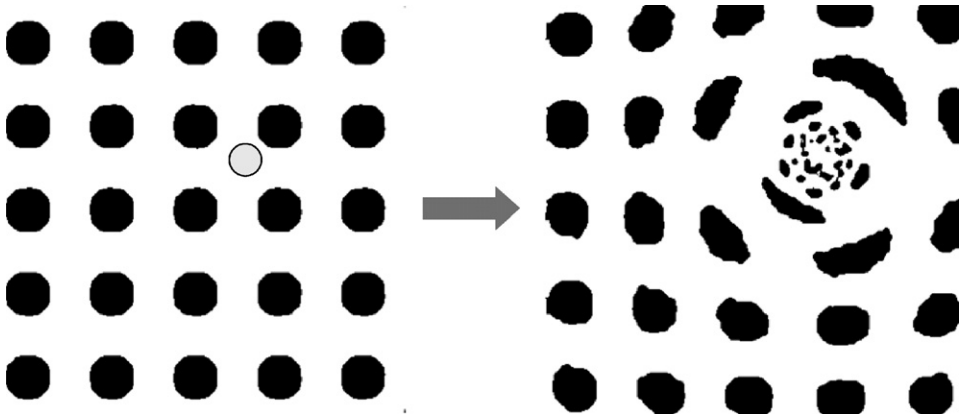

Fig. 1. Schematic illustration of strong gravitational lensing. Left: an array of background sources (black) with the position of a foreground lens (gray circle). Right: the image seen by an observer after gravitational lensing. In LSST images, foreground mass overdensities will induce correlated distortions of galaxy shapes at the 10^{-4} level.

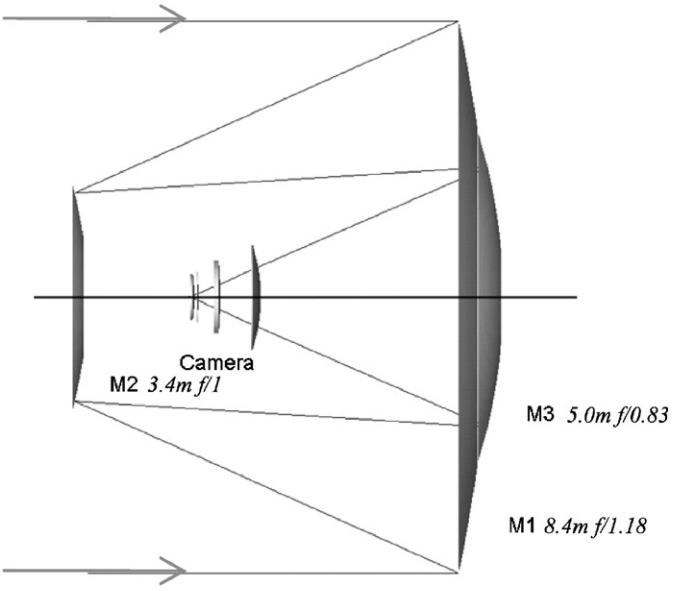

Fig. 2. Optical design of the Large Synoptic Survey Telescope.

Table 1
Key science goals of the LSST camera and corresponding sensor requirements

Science goal	Sensor requirement
High QE to $\lambda = 1000$ nm	Thick silicon (>75 μm)
Point spread function $\ll 0.7$ arcsec	Small pixel size (0.2 arcsec = 10 μm) High internal field in sensor ($\sim$5 kV/cm) High-resistivity silicon ($>$5k9 cm)
Fast f/1.2 focal ratio	Sensor flatness <5 μm pk-pk
Wide field of view (3.5°)	$\sim$3200 cm^2 focal plane $\sim$200-CCD mosaic ($\sim$16 cm^2 each) Industrialized production process required
High throughput	>90% fill factor Four-side buttable package with sub-millimeter gaps
Fast readout (2 s) with low read noise (5 e$^-$ rms)	Segmented sensors ($\sim$3200 total output ports) 16 I/O ports per CCD

periodic calibration of the instrument and atmosphere will ensure accurate photometry. Each field will be imaged more than 200 times during the survey with each of five filters, so that a particular astronomical source is imaged each time through a different atmosphere, on a different set of detector pixels, and at different telescope attitude. In this way systematic image distortions, which contaminate the weak lensing signal will be averaged out.

In addition to its primary goal of studying dark energy via weak lensing and the other techniques discussed above, LSST's science missions include

- solar system inventory—Trans-Neptunian objects and potentially hazardous asteroids;
- exploring the transient optical sky—supernovae, optical bursters, and variables over timescales from minutes to tens of years; and
- mapping the Milky Way—positions and proper motions of all stars within 300 pc of the Sun, stellar kinematics.

4. The LSST camera

The LSST camera is optimized for a wide field of view (3.5° diameter, focal ratio f/1.2), angular resolution limited by atmospheric turbulence (0.6 arcsec median seeing at the selected site), wide wavelength range (350–1100 nm), and fast readout (under 3 s). In addition to the focal plane, it contains three large lenses, a shutter, and a mechanism for exchanging filters. A diagram of the major camera components is shown in Fig. 3. The heart of the camera is the cryostat containing the science sensors, as well as wavefront and guide sensors. The 63-cm diameter focal plane must be tiled with a large number (about 200) of CCD sensors operating at a temperature of around -100 °C. Access constraints require most of the support electronics to be located directly behind the focal plane, inside the cryostat. To streamline assembly and maintenance, the sensors and electronics are constructed in "raft towers", modules of 3×3 CCDs with a tightly integrated front-end electronics package. The proposed layout of the focal plane is illustrated in Fig. 4, and a depiction of the raft tower is shown in Fig. 5.

5. Sensors

The science goals of LSST place a set of challenging requirements on the focal plane array sensors. Present-generation astronomical CCDs feature back illumination, large formats up to 2K $\times$ 4K with 12–15 μm pixels, silicon thickness 10–40 μm, and 1, 2, or 4 outputs. Large mosaic cameras up to $\sim$300 Mpixels have been constructed as mosaics of $\sim$40 cooled CCDs, with all readout electronics located outside the cryostat; a review can be found in Ref. [6]. Three important improvements are foreseen for LSST sensors, described in the following sections.

5.1. Extended red response with low diffusion

To detect and tag high-redshift galaxies, the sensors should have high quantum efficiency not only in the visible but also in the near-IR. To extend the sensors' QE to wavelengths near the bandgap of silicon, the total silicon thickness must be greater than in present-generation CCDs; at least 200 μm of Si are needed to achieve 50% QE at 1000 nm at low temperature. However, spreading of photogenerated carriers by diffusion through the thick Si layer degrades the image quality. To overcome this drawback, the sensor must be fabricated from high resistivity silicon (>5 kΩ cm) and must have a bias voltage applied between the entrance window and the electrode

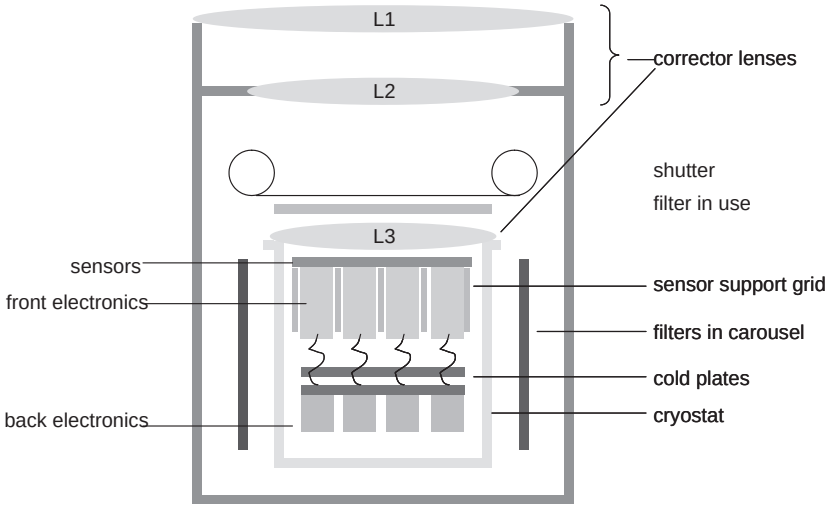

Fig. 3. Components of the LSST camera.

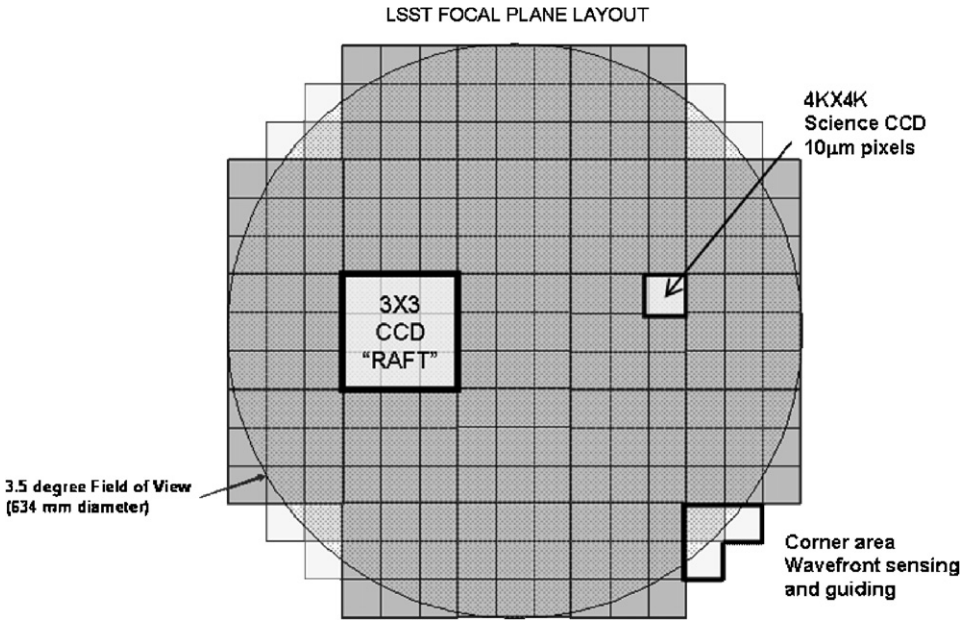

Fig. 4. Focal plane layout showing raft modules.

side. With a high enough applied bias, the entire layer will be depleted of free carriers and a high electric field will exist throughout the silicon thickness. For a sufficient degree of overdepletion, photogenerated electrons will drift at nearly their saturated velocity; the transit time across the thick silicon layer will be minimized, reducing diffusion spread. CCDs that use thick, fully depleted, high resistivity silicon to achieve enhanced red response have been demonstrated in the laboratory [7–9].

The present CCD design calls for a silicon layer of 10 kΩ cm resistivity, 100 μm thick, operated at 173 K with an applied electric field of 5 kV/cm. Under these conditions one expects an internal QE of about 28% at 1000 nm wavelength, and diffusion of 2.9 μm rms. This corresponds to a point spread function (PSF) with a full-width at half-maximum of about 0.14 arcsec, which should be compared to the 0.6 arcsec median atmospheric seeing and 0.24 arcsec from the optical design (including fabrication and alignment tolerances). With a pixel size of 10 μm, these sensors will contribute negligibly to LSST's image quality budget even in the best atmospheric seeing conditions.

A detailed study of thickness optimization for LSST sensors has been performed and is summarized in Ref. [10]. Selected results for QE and PSF are shown in Figs. 6 and 7.

5.2. *Fast, parallel readout*

LSST's survey efficiency depends on the telescope's ability to rapidly move from field to field on the sky during a night's observing. The mount has been engineered to slew

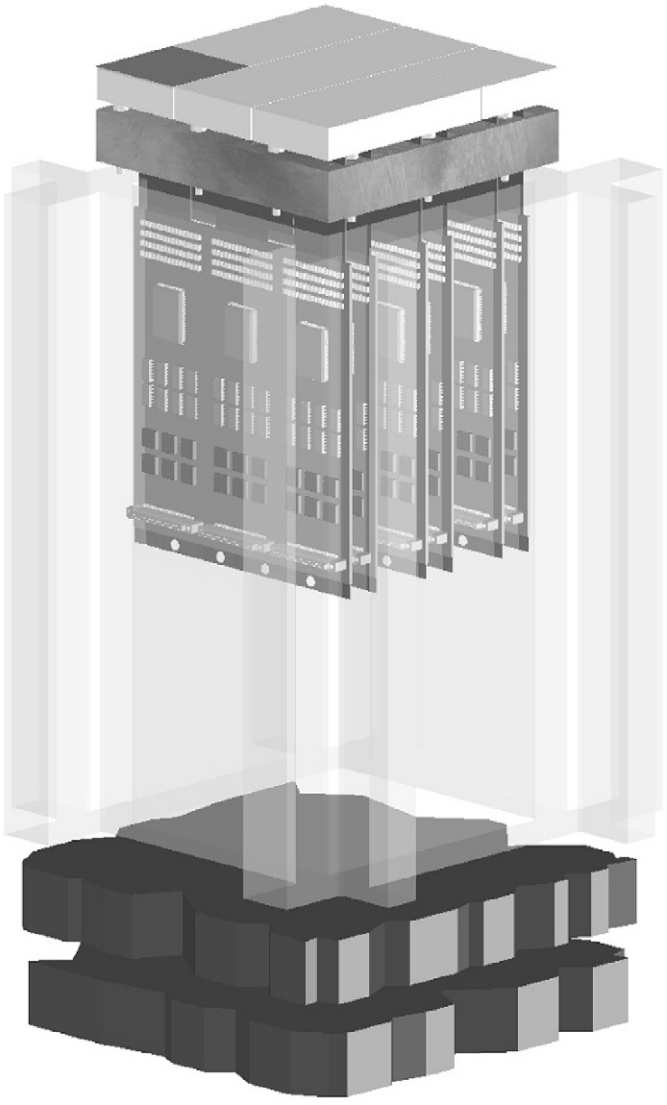

Fig. 5. Raft tower, the modular unit of the LSST focal plane. Sensors (top) rest on a passive base immediately in front of the front-end electronics package. Supporting grid and cooling plates are also shown. Twenty-one raft towers populate the full 3.2 Gpixel focal plane.

and settle within 5 s. During this time, the shutter is closed and the camera must read out the complete 3.2 Gpixel image acquired in the previous field. By comparison, present-generation mosaic cameras take 30–60 s to read out their 300 Mpixel focal planes. LSST has therefore adopted a highly parallel architecture, with each $4K \times 4K$ sensor subdivided into 16 independently readout segments. The layout of these segments, illustrated in Fig. 8, results in 16 contiguous imaging areas of 2000 rows $\times$ 500 columns. These will be read out in parallel at about 500 kpixels/s to meet a goal of 2 s total readout time. It is expected that a sensor layout of this type can achieve $>90\%$ fill factor.

5.3. Precise mechanical packaging

The optical system of the LSST has a fast $f/1.2$ focal ratio to achieve an extremely wide 3.5° diameter field of view; unfortunately, such a wide field design results in a very limited depth of focus. The sensors therefore have to be fabricated so that they will have no more than 5 μm deviation from flatness after thinning and packaging. Moreover, their packages must be produced with tight dimensional tolerance to allow for parallel, height-matched assembly onto the mosaic baseplate. Mounting alignment must be maintained over a 100 °C cool-down range and over orientation changes of the camera. Various design concepts using adjustable three-point mounts are being investigated. The assembled focal plane mosaic must preserve as high a fill factor as possible, requiring sub-millimeter gaps between sensors and rafts.

6. Electronics

The highly parallel electronics architecture of the LSST is complicated by the location of the focal plane array inside a vacuum cryostat. We have chosen a design where the amplification, sampling, digitizing, and multiplexing functions are implemented in compact ASICs located in two thermal zones within the cryostat. The front end analog signal processing for 144 channels are located in a $120 \times 120 \times 180\,\mathrm{mm}^3$ card cage directly behind the raft baseplate holding the CCDs. This section operates close to the sensor temperature. Analog flex cables transmit signals to the digitizing and multiplexing back end which resides in a similar sized bay, still within the cryostat but at a warmer temperature. After multiplexing, the digital data exits the cryostat via 1.25 Gb/s optical fibers, one per raft. For obvious reasons the power dissipation within the cryostat must be kept as low as possible. A signal processing ASIC, incorporating dual slope integrators for correlated double sampling, and a clock and bias generator ASIC in high-voltage technology, are now in design. It is expected that with these ASICs plus modern ADCs and FPGAs the in-cryostat electronics should dissipate no more than 100 mW/channel (320 W total). This should be compared with 115 W heat load contributed by radiation from the vacuum window onto the focal plane array.

Analog electronics are required to have a wide dynamic range and very low channel-to-channel crosstalk. The CCDs will have a readout noise of $\sim 5e^-$ and a full-scale signal of $100{,}000e^-$. Modern submicron CMOS has superior performance at low temperature and can meet or exceed the noise and dynamic range requirement. However, control of crosstalk at the sensor, ASIC, and board level poses significant challenges, particularly in view of the low supply voltage of CMOS. Differential signaling and careful attention to shielding and power supply decoupling will be used to control crosstalk, but software correction of the residual crosstalk will still be needed.

7. Comparison with collider detectors

The LSST camera bears certain similarities to silicon-based tracking detectors used in large colliders. Both are

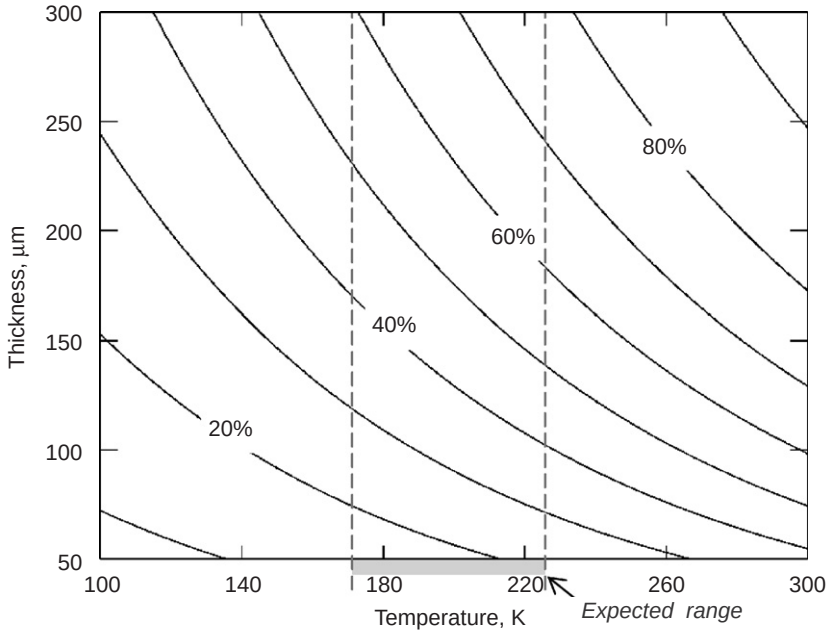

Fig. 6. Internal quantum efficiency at 1 µm wavelength, shown as a function of silicon thickness and temperature [10]. LSST requirement is 25% QE with a goal of 45%.

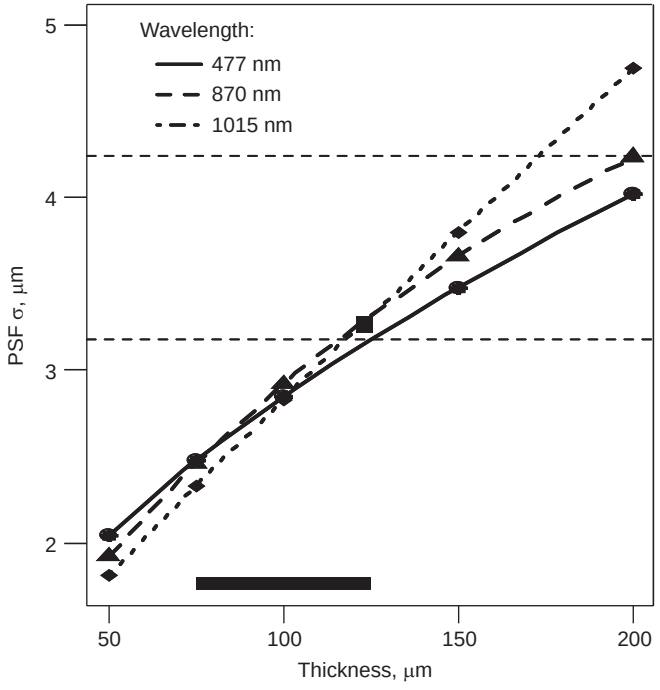

Fig. 7. Point spread function (modeled) vs. thickness and wavelength for an *n*-channel CCD operated at 5 kV/cm internal electric field [10].

intended for use in experiments that probe new fundamental physics. Management, transport, and distribution of data at the Petabyte scale are needed in each case. With their fine pixilation, extensive use of silicon sensors and integrated electronics, and dependence on a huge beam-delivery system, both detectors require a large team of technical specialists to address their unique requirements. Modular construction is chosen in both cases to aid assembly and integration. Table 2 presents a comparison of some of the high-level features of the LSST and the tracking detectors built for the LHC. The main features to note are that although LSST is much smaller in area than the collider detectors, it has finer pixilation, higher dynamic range, and 100% "occupancy". Individual "events" (images) occur at a much slower rate than in the colliders, but have much more information content per frame resulting in a similar overall rate of data generation.

8. Conclusion

The LSST's high-throughput design will provide a spectacular advance in astronomical data-gathering capability. Many of the most challenging aspects of this design are in the sensors and electronics that make up the 3.2 Gpixel focal plane array of the LSST's wide-field camera. A number of R&D investigations are now underway with the goal of resolving all the technical questions relating to achieving extended red response, small point spread function, fast parallel readout, low power dissipation, and precision mosaic assembly.

With new-generation optics, camera, and computing, the LSST observatory will provide the raw data needed to respond to the compelling questions raised by recent discoveries in astroparticle physics and cosmology.

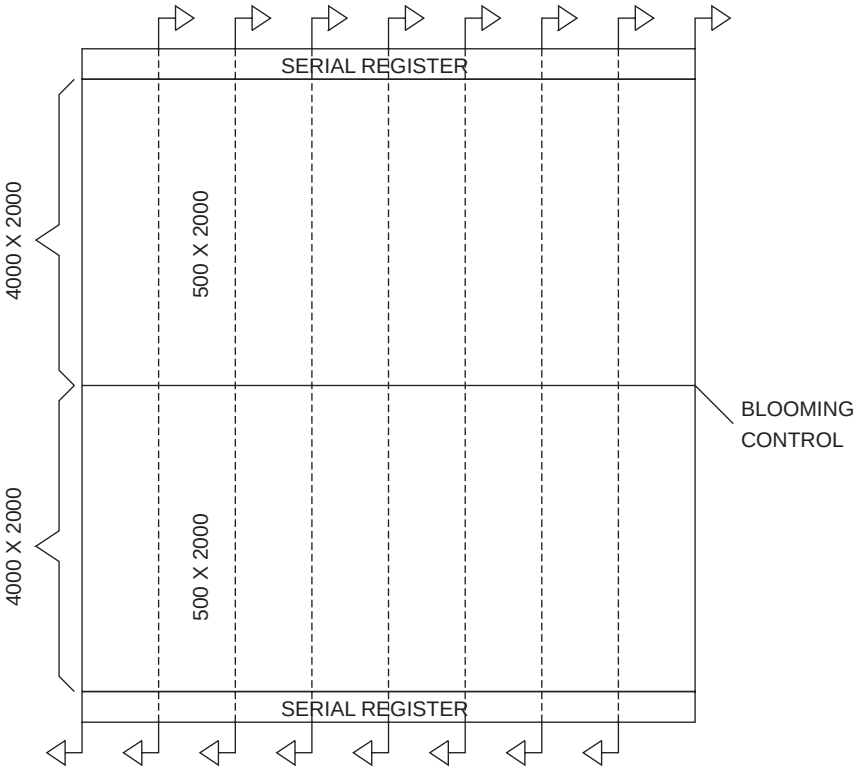

Fig. 8. Layout of the proposed 16 Mpixel LSST CCD. Each CCD is segmented into 16 subsections, which can be read out in parallel. This parallelism allows the entire focal plane to be read out in 2 s without resorting to high clock rates, which tend to increase noise and crosstalk.

Table 2
High-level comparison of LSST and LHC detectors

	LHC tracker	LSST
Acceptance	4π "in"	2π "out"
Elx. channels	10^8	3200
Si area (m^2)	10^2	0.3
Alignment priority	x–y–θ	z
Max S/N	30	20,000
Occupancy (%)	few	100
Trigger rate (Hz)	10^5	0.06
Readout rate (MHz)	40	500
Data volume	100 MB	6 GB
Structure	Static	Dynamic
Environmental concerns	Radiation	Wind, lightning, outgassing

Acknowledgments

Manuscript was authored by employees of Brookhaven Science Associates, LLC under contract DE-AC02-98CH10886 with the US Department of Energy. The LSST design and development activity are supported by the National Science Foundation under Scientific Program order no. 9 (AST-0551161) through Cooperative Agreement AST-0132798. Portions of this work were performed in part under Department of Energy contracts DE-AC02-76SF00515, DE-FG02-91ER40677 and W-7405-Eng-48. Additional funding comes from private donations, in-kind support at Department of Energy laboratories and other LSSTC Institutional Members.

References

[1] D.N. Spergel, et al., Astrophys. J. Supp. 170 (2007) 377.
[2] S. Perlmutter, et al., Astrophys. J. 517 (1999) 565.
[3] M. Bartelmann, P. Schneider, Phys. Rep. 340 (2001) 291.
[4] D.J. Eisenstein, et al., Astrophys. J. 633 (2005) 560.
[5] J.A. Tyson, et al., Nucl. Phys. B—Proc. Suppl. 124 (2003) 21 (see also ⟨http://www.lsst.org⟩).
[6] P. Jorden, D. Murray, P. Poole, SPIE 5167 (2004) 72.
[7] S. Holland, D. Groom, N. Palaio, R. Stover, M. Wei, IEEE Trans. Nucl. Sci. NS50 (1) (2003) 225.
[8] Y. Kamata, et al., Proc. SPIE, June 2006, (6276-73).
[9] P. Jorden, et al., Proc. SPIE, June 2006, (6276-04).
[10] P. O'Connor, et al., Proc. SPIE, June 2006, (6276-75).